Hindawi
Mathematical Problems in Engineering
Volume 2019, Article ID 5325817, 7 pages
https://doi.org/10.1155/2019/5325817

*Research Article*

# Highly Accurate Multi-Invariance ESPRIT for DOA Estimation with a Sparse Array

**Chen Gu,[1] Hong Hong,[1] Yusheng Li,[1] Xiaohua Zhu,[1] and Jin He[2]**

[1]*Department of Electronic Engineering, Nanjing University of Science and Technology, 210094 Nanjing, Jiangsu, China*
[2]*Shanghai Key Laboratory of Intelligent Sensing and Recognition, School of Electronic Information and Electrical Engineering, Shanghai Jiaotong University, Shanghai, 200240, China*

Correspondence should be addressed to Jin He; jinhe@sjtu.edu.cn

Received 21 August 2018; Revised 19 December 2018; Accepted 4 February 2019; Published 18 February 2019

Academic Editor: Krzysztof S. Kulpa



This paper proposes a multi-invariance ESPRIT-based method for estimation of 2D direction (MIMED) of multiple non-Gaussian monochromatic signals using cumulants. In the MIMED, we consider an array geometry containing sparse $L$-shaped diversely polarized vector sensors plus an arbitrarily-placed single polarized scalar sensor. Firstly, we define a set of cumulant matrices to construct two matrix blocks with multi-invariance property. Then, we develop a multi-invariance ESPRIT-based algorithm with aperture extension using the defined matrix blocks to estimate two-dimensional directions of the signals. The MIMED can provide highly accurate and unambiguous direction estimates by extending the array element spacing beyond a half-wavelength. Finally, *we present* several simulation results to demonstrate the superiority of the MIMED.

## 1. Introduction

Estimation of direction-of-arrival (DOA) and polarization parameters using an array of diversely polarized electromagnetic vector sensors is very important in many applications, such as radar and wireless communications. In the past two decades, many electromagnetic vector sensor direction finding algorithms have been proposed [1–8]. Among them, ESPRIT-based algorithms [2–4] are highly popular due to their low computations and high estimation accuracy. Generally, the ESPRIT-based algorithm exploits the spatial invariance between two identical subarrays to offer direction estimation.

Multi-invariance ESPRIT (MI-ESPRIT), first proposed in [9], is an extension of conventional ESPRIT by exploiting the inherent multiple invariances embedded in the array structure. With exploitation of the special multi-invariance structure, MI-ESPRIT can offer better estimation performance than original version of ESPRIT [9]. *In recent years, MI-ESPRIT algorithm has been applied to solve direction finding problems, where the impinging signals can be MC-CDMA [10], Noncircular [11], and narrowband chirp [12]*. However, all the MI-ESPRIT-based algorithms mentioned above are developed using scalar arrays, with array intersensor spacing being not beyond a half-wavelength to guarantee unique and unambiguous direction estimates.

In this paper, we apply the idea of MI-ESPRIT to sparse electromagnetic vector sensor arrays to achieve aperture extension for highly accurate direction estimation. We present a multi-invariance ESPRIT-based method for estimation of two-dimensional direction (MIMED) of multiple non-Gaussian signals using cumulants. In the proposed MIMED, we consider an array geometry that contains sparse $L$-shaped diversely polarized vector sensors plus an arbitrarily-placed single polarized scalar sensor (dipole). Firstly, a set of cumulant matrices is defined to form two matrix blocks that possess the multi-invariance property. Then, a multi-invariance ESPRIT-based algorithm with aperture extension using the defined matrix blocks to estimate two-dimensional directions of the signals is developed. The MIMED can provide highly accurate and unambiguous angle estimates by exploiting *the fact that the spatial phase factor* is larger than a half-wavelength.

Note also that the MIMED algorithm is related to the algorithm presented in [13] in the sense that both algorithms define the cumulant matrices to estimate the directions of

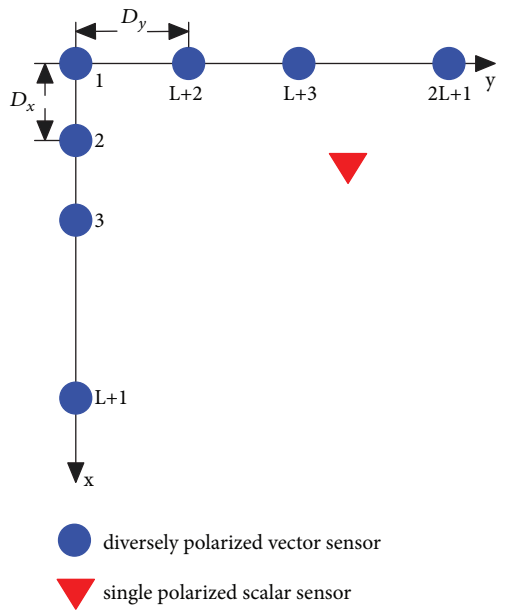


FIGURE 1: Array configuration for the MIMED: $\overline{L} = 2L + 1$ sparse $L$-shaped diversely polarized vector sensors plus an arbitrarily-placed single polarized scalar sensor.

signals. However, since the sensors used in the MIMED algorithm are different from those in [13], the algorithmic derivation and performance bounds are different from those in [13]. For example, (i) [13] is derived based on a scalar sensor array, whereas the MEMID algorithm is derived using a vector sensor array; (ii) the algorithm in [13] defines cumulant matrices to formulate the tensor model, whereas the MIMED algorithm defines cumulant matrices to form the multi-invariance ESPRIT model.

*Notation*. Throughout the paper, superscripts $T$, $H$, $*$, and $\dagger$, respectively, represent the transpose, conjugate transpose, complex conjugate, and pseudoinverse, and $\otimes$ denotes the Kronecker-product operator. $\lceil x \rceil$ denotes the smallest integer not less than $x$, $\lfloor x \rfloor$ represents the largest integer not greater than $x$, and $\arg\{z\}$ signifies the principal argument of the complex number $z$ between $-\pi$ and $\pi$.

## 2. Signal Model

Consider $M$ narrowband completely polarized source signals, parameterized by $\{\theta_1, \phi_1, \gamma_1, \eta_1\}$, $\{\theta_2, \phi_2, \gamma_2, \eta_2\}$, $\ldots, \{\theta_M, \phi_M, \gamma_M, \eta_M\}$, *where* $0 \le \theta_m < \pi$, $0 \le \phi_m < 2\pi$, $0 \le \gamma_m < \pi/2$, *and* $-\pi \le \eta_m < \pi$, *respectively, denote the elevation angle, azimuth angle, orientation angle, and ellipticity angle of the mth source,* impinging upon an array, which is composed of $\overline{L} = 2L + 1$ sparse $L$-shaped diversely polarized vector sensors plus an arbitrarily-placed single polarized scalar sensor, as shown in Figure 1. The location of the $\ell$th ($\ell = 1, \ldots, L + 1$) sensor lied on the $x$-axis is $((\ell - 1)D_x, 0)$, and the location of the $k$th ($k = L + 2, \ldots, \overline{L}$) sensor lied on the $y$-axis is $(0, (k - L - 1)D_y))$, where $D_x \gg \lambda$ and $D_y \gg \lambda$ are the intersensor spacing. Each electromagnetic vector sensor consists of six spatially orthogonal but colocated components: three electric dipoles plus three magnetic loops. The electromagnetic vector sensor response for the $m$th source signal produces the following $6 \times 1$ steering vector [2]:

$$\boldsymbol{c}_m = \boldsymbol{c}(\theta_m, \phi_m, \gamma_m, \eta_m) = \begin{bmatrix} c_1(\theta_m, \phi_m, \gamma_m, \eta_m) \\ c_2(\theta_m, \phi_m, \gamma_m, \eta_m) \\ c_3(\theta_m, \phi_m, \gamma_m, \eta_m) \\ c_4(\theta_m, \phi_m, \gamma_m, \eta_m) \\ c_5(\theta_m, \phi_m, \gamma_m, \eta_m) \\ c_6(\theta_m, \phi_m, \gamma_m, \eta_m) \end{bmatrix}$$

$$\stackrel{\text{def}}{=} \begin{bmatrix} e_x(\theta_m, \phi_m, \gamma_m, \eta_m) \\ e_y(\theta_m, \phi_m, \gamma_m, \eta_m) \\ e_z(\theta_m, \gamma_m, \eta_m) \\ h_x(\theta_m, \phi_m, \gamma_m, \eta_m) \\ h_y(\theta_m, \phi_m, \gamma_m, \eta_m) \\ h_z(\theta_m, \gamma_m) \end{bmatrix} \tag{1}$$

$$= \begin{bmatrix} \sin\gamma_m \cos\theta_m \cos\phi_m e^{j\eta_m} - \cos\gamma_m \sin\phi_m \\ \sin\gamma_m \cos\theta_m \sin\phi_m e^{j\eta_m} + \cos\gamma_m \cos\phi_m \\ -\sin\gamma_m \sin\theta_m e^{j\eta_m} \\ -\cos\gamma_m \cos\theta_m \cos\phi_m - \sin\gamma_m \sin\phi_m e^{j\eta_m} \\ -\cos\gamma_m \cos\theta_m \sin\phi_m + \sin\gamma_m \cos\phi_m e^{j\eta_m} \\ \cos\gamma_m \sin\theta_m \end{bmatrix}$$

where the first three entries ($\boldsymbol{e}_m = [e_{x,m}, e_{y,m}, e_{z,m}]^T$) and the last three entries ($\boldsymbol{h}_m = [h_{x,m}, h_{y,m}, h_{z,m}]^T$) represent the electric and the magnetic field vectors, respectively. Note that the array manifold of electromagnetic vector sensors does not *contain the angle-related phase factor*. This fact is pivotal to the MIMED in improving the estimation accuracy by extending the array aperture beyond that limited by the spatial Nyquist sampling theorem. Also, note that the Frobenius-norm of the normalized Poynting vector is independent of the parameters of the signal and is equal to unity. That is, the electric field vector $\mathbf{e}_m$ and the magnetic field vector $\mathbf{h}_m$ are orthogonal to each other and to the source signal's normalized Poynting vector $\mathbf{p}_m$, i.e., [2]

$$\boldsymbol{p}_m \stackrel{\text{def}}{=} \boldsymbol{e}_m \times \boldsymbol{h}_m^H \stackrel{\text{def}}{=} \begin{bmatrix} u_m \\ v_m \\ w_m \end{bmatrix} \stackrel{\text{def}}{=} \begin{bmatrix} \sin\theta_m \cos\phi_m \\ \sin\theta_m \sin\phi_m \\ \cos\theta_m \end{bmatrix} \tag{2}$$

where $u_m$, $v_m$, and $w_m$ denote the direction cosines of the $x$-axis, $y$-axis, and $z$-axis.

Then, the $6(L+1)\times 1$ data vectors measured by the first to *the* $(L+1)$*th vector sensors* at time $t$ can be expressed as

$$\begin{aligned}\boldsymbol{z}_x(t) &= \sum_{m=1}^{M}\left(\boldsymbol{q}_x(\theta_m,\phi_m)\otimes \mathbf{c}_m\right)s_m(t)+\boldsymbol{n}_x(t)\\ &= \boldsymbol{A}_x\boldsymbol{s}(t)+\boldsymbol{n}_x(t)\end{aligned} \tag{3}$$

where $s_m(t)$ denotes the phasor representation of the $m$th signal, $\boldsymbol{s}(t) = [s_1(t),\ldots,s_M(t)]^T$ denotes the signal vector, $\boldsymbol{A}_x = [\boldsymbol{q}_x(\theta_1,\phi_1)\otimes\boldsymbol{c}_1,\ldots,\boldsymbol{q}_x(\theta_M,\phi_M)\otimes\boldsymbol{c}_M]$, with $\boldsymbol{q}_x(\theta_m,\phi_m) = [1, e^{j2\pi/\lambda D_x u_m},\ldots,e^{j2\pi/\lambda(L-1)D_x u_m}]^T$, and $\boldsymbol{n}_x(t)$ represent the $6(L+1)\times 1$ additive noise vector. Likewise, the $6L\times 1$ output vector measured by *the* $(L+2)$*th* to $\overline{L}$th vector sensors can be expressed as

$$\begin{aligned}\boldsymbol{z}_y(t) &= \sum_{m=1}^{M}\left(\boldsymbol{q}_y(\theta_m,\phi_m)\otimes \mathbf{c}_m\right)s_m(t)+\boldsymbol{n}_y(t)\\ &= \boldsymbol{A}_y\boldsymbol{s}(t)+\boldsymbol{n}_y(t)\end{aligned} \tag{4}$$

where $\boldsymbol{A}_y = [\boldsymbol{q}_y(\theta_1,\phi_1)\otimes\boldsymbol{c}_1,\ldots,\boldsymbol{q}_y(\theta_M,\phi_M)\otimes\boldsymbol{c}_M]$, with $\boldsymbol{q}_y(\theta_m,\phi_m) = [e^{j2\pi/\lambda D_y v_m},\ldots,e^{j2\pi/\lambda(L-1)D_y v_m}]^T$, and $\boldsymbol{n}_y(t)$ represent the $6L\times 1$ additive noise vector.

Next, we assume the single polarized scalar sensor is placed arbitrarily at the location $(d_x, d_y)$. Then, the data collected by the single polarized scalar sensor can be represented as

$$z_0(t) = \sum_{m=1}^{M} q_0(\theta_m,\phi_m)\,s_m(t)+n_0(t) \tag{5}$$

where $q_0(\theta_m,\phi_m) = e^{j2\pi/\lambda(d_x u_m + d_y v_m)}$ and $n_0(t)$ is additive noise.

With a total of $N$ snapshots taken at $\{t_n : n = 1,\ldots,N\}$, the problem is to determine the azimuth-elevation directions $\{\theta_m,\phi_m,\ m = 1,\ldots,K\}$ from these snapshots. For beamforming purposes, it may be also useful to subsequently estimate the corresponding polarization parameters $\{\gamma_m,\eta_m,\ m = 1,\ldots,K\}$. We will present the MIMED algorithm to solve the above-mentioned problems in Section 3, under the following assumptions: (i) the parameters $(\theta_1,\phi_1,\gamma_1,\eta_1),\ldots,(\theta_M,\phi_M,\gamma_M,\eta_M)$ are distinct with each other, and the array steering vector matrix is of full column rank; (ii) the impinging signals are zero-mean and stationary, mutually independent, and non-Gaussian, having nonzero fourth-order cumulants; (iii) the noise is zero-mean, complex Gaussian, and possibly spatially correlated.

## 3. Algorithm Development

*3.1. Formulation of the Cumulant Matrices.* In this subsection, we define $2L+1$ cumulant matrices that can be linked to multi-invariance model for direction estimation. In forming the cumulant matrices, the single polarized scalar sensor is used as a reference sensor. Let $z_{i,\imath}(t)$, $z_{j,\jmath}(t)$, and $z_{p,\kappa}(t)$ be the data measured by the $\imath$th, $\jmath$th, and $\kappa$th $(\imath,\jmath,\kappa = 1,\ldots,6)$ vector sensor element from the $L$-shaped vector sensors, and let the fourth-order cumulants of $z_0(t)$, $z_{i,\imath}(t)$, $z_{j,\jmath}(t)$, and $z_{p,\kappa}(t)$ be $\mathrm{cum}(z_0(t), z^*_{i,\imath}(t), z_{j,\jmath}(t), z^*_{p,\kappa}(t))$. Using the assumptions made in Section 2 and the cumulant properties in [14], we have

$$\begin{aligned}&\mathrm{cum}\left(z_0(t), z^*_{i,\imath}(t), z_{j,\jmath}(t), z^*_{p,\kappa}(t)\right)\\ &\quad= \sum_{m=1}^{M}\zeta_m c^*_\imath(\theta_m,\phi_m,\gamma_m,\eta_m)\,e^{j(2\pi/\lambda)(x_{0,i,j,p}u_m + y_{0,i,j,p}v_m)}\end{aligned} \tag{6}$$

where $i, j, p \in \{1,\ldots,2L+1\}$ and

$$\begin{aligned}x_{0,i,j,p} &= d_x - x_i + x_j - x_p\\ y_{0,i,j,p} &= d_y - y_i + y_j - y_p\end{aligned} \tag{7}$$

with $(x_i, y_i)$ being the location of the $i$th vector sensor, and

$$\zeta_m = \mathrm{cum}\left(s_m(t), s^*_m(t), s_m(t), s^*_m(t)\right) = E\left\{\left|s_m(t)\right|^4\right\} \tag{8}$$

Then, denoting the $6\overline{L}\times 1$ vector $\boldsymbol{z}(t) = [\boldsymbol{z}_x^T(t), \boldsymbol{z}_y^T(t)]^T$, we define the $\overline{L}$ $6\overline{L}\times 6\overline{L}$ cumulant matrices as

$$\begin{aligned}\boldsymbol{R}_\ell &= \sum_{k=1}^{6}\mathrm{cum}\left(z_0(t), z^*_{\ell,k}(t), \boldsymbol{z}(t), \boldsymbol{z}^H(t)\right),\\ &\qquad\qquad \ell = 1,\ldots,\overline{L}\end{aligned} \tag{9}$$

where $z_{\ell,k}(t)$ is the $k$th row of $\boldsymbol{z}_\ell(t)$. After some mathematical computations, we can obtain

$$\boldsymbol{R}_1 = \boldsymbol{A}\boldsymbol{G}\boldsymbol{A}^H \tag{10}$$

$$\boldsymbol{R}_\ell = \boldsymbol{A}\boldsymbol{\Phi}_u^{\ell-1}\boldsymbol{G}\boldsymbol{A}^H,\quad \ell = 2,\ldots,L+1 \tag{11}$$

$$\boldsymbol{R}_{\overline{\ell}} = \boldsymbol{A}\boldsymbol{\Phi}_v^{\overline{\ell}-L-1}\boldsymbol{G}\boldsymbol{A}^H,\quad \overline{\ell} = L+2,\ldots,2L+1 \tag{12}$$

where

$$\begin{aligned}\boldsymbol{G} = \mathrm{diag}\Bigg\{&\zeta_1\sum_{k=1}^{6}c^*_k(\boldsymbol{\theta}_1)\,e^{j2\pi/\lambda(d_x u_1 + dy v_1)},\ldots,\\ &\zeta_M\sum_{k=1}^{6}c^*_k(\boldsymbol{\theta}_M)\,e^{j2\pi/\lambda(d_x u_M + dy v_M)}\Bigg\}\end{aligned} \tag{13}$$

$$\boldsymbol{\Phi}_u = \mathrm{diag}\left\{e^{j2\pi/\lambda D_x u_1},\ldots,e^{j2\pi/\lambda D_x u_M}\right\} \tag{14}$$

$$\boldsymbol{\Phi}_v = \mathrm{diag}\left\{e^{j2\pi/\lambda D_y v_1},\ldots,e^{j2\pi/\lambda D_y v_M}\right\} \tag{15}$$

with $\boldsymbol{\theta}_m = (\theta_m,\phi_m,\gamma_m,\eta_m)$.

Next, we construct two $6(L+1)\overline{L}$ data blocks using the defined cumulant matrices as

$$\boldsymbol{R}_x = \begin{bmatrix} \boldsymbol{R}_1 \\ \boldsymbol{R}_2 \\ \vdots \\ \boldsymbol{R}_{L+1} \end{bmatrix}, \quad \boldsymbol{R}_y = \begin{bmatrix} \boldsymbol{R}_1 \\ \boldsymbol{R}_{L+2} \\ \vdots \\ \boldsymbol{R}_{2L+1} \end{bmatrix} \tag{16}$$

With the foregoing definitions, we will show in next subsection that $\boldsymbol{R}_x$ and $\boldsymbol{R}_y$ are of multi-invariance properties, which can be exploited to estimate the directions of signals using MI-ESPRIT algorithm.

*3.2. MI-ESPRIT Algorithm for Direction Estimation.* It is easily to verify that the block $\boldsymbol{R}_x$ is of the form

$$\boldsymbol{R}_x = \begin{bmatrix} \boldsymbol{R}_1 \\ \boldsymbol{R}_2 \\ \vdots \\ \boldsymbol{R}_{L+1} \end{bmatrix} = \begin{bmatrix} \boldsymbol{A} \\ \boldsymbol{A}\boldsymbol{\Phi}_u \\ \vdots \\ \boldsymbol{A}\boldsymbol{\Phi}_u^L \end{bmatrix} \boldsymbol{G}\boldsymbol{A}^H \tag{17}$$

The first $\overline{L}$ rows of $\boldsymbol{R}_x$ can be considered as measurement of signal $\boldsymbol{G}\boldsymbol{A}^H$ by physical vector sensors, while the $i$th $\overline{L}$ rows ($(i-1)\overline{L}+1$ to $i\overline{L}$ rows) of $\boldsymbol{R}_x$ can be viewed as measurement of signal $\boldsymbol{G}\boldsymbol{A}^H$ by virtual vector sensors, *which are virtually placed* by shifting the physical sensors along $x$-axis with distance $(i-1)D_x$. Then, for all $i = 2, \ldots, L+1$, altogether $L$ different virtual sensor groups can be formed. Each virtual sensor group has its own spatial invariance, so that $L$ distinct spatial invariances can be provided [9]. Therefore, the matrix (17) is of multi-invariance characteristic [9] which can be exploited for use of MI-ESPRIT for estimating directions. The signal subspace matrix $\boldsymbol{E}_{s,x}$, which contains the eigenvectors associated with $M$ largest eigenvalues of $\boldsymbol{R}_x\boldsymbol{R}_x^H$, can be represented as

$$\boldsymbol{E}_{s,x} = \begin{bmatrix} \boldsymbol{A} \\ \boldsymbol{A}\boldsymbol{\Phi}_u \\ \vdots \\ \boldsymbol{A}\boldsymbol{\Phi}_u^L \end{bmatrix} \boldsymbol{T} \tag{18}$$

where $\boldsymbol{T}$ is an $M \times M$ full rank matrix.

Let $\boldsymbol{E}_{s,x,1}$ and $\boldsymbol{E}_{s,x,2}$, respectively, be the first $6L\overline{L}$ rows and the last $6L\overline{L}$ rows of $\boldsymbol{E}_{s,x}$; we have

$$\boldsymbol{E}_{s,x,2} = \boldsymbol{E}_{s,x,1}\boldsymbol{T}^{-1}\boldsymbol{\Phi}_u\boldsymbol{T} \tag{19}$$

From (19), we can infer that, with the estimation of $\widehat{\boldsymbol{E}}_{s,x,1}$ and $\widehat{\boldsymbol{E}}_{s,x,2}$, the diagonal elements of $\boldsymbol{\Phi}_u$ can be estimated from eigenvalues of $\widehat{\boldsymbol{E}}_{s,x,1}^{\dagger}\widehat{\boldsymbol{E}}_{s,x,2}$ and the matrix $\boldsymbol{T}$ can be estimated from the eigenvectors of $\widehat{\boldsymbol{E}}_{s,x,1}^{\dagger}\widehat{\boldsymbol{E}}_{s,x,2}$, i.e.,

$$\widehat{\boldsymbol{E}}_{s,x,1}^{\dagger}\widehat{\boldsymbol{E}}_{s,x,2} = \widehat{\boldsymbol{T}}^{-1}\widehat{\boldsymbol{\Phi}}_u\widehat{\boldsymbol{T}} \tag{20}$$

where $\{[\widehat{\boldsymbol{\Phi}}_u]_{m,m} = e^{j2\pi/\lambda D_x \widehat{u}_m},\ m = 1, 2, \ldots, M\}$. Since $D_x > \lambda/2$, a set of ambiguous direction cosine estimates $u_m$ that satisfy (20) can be obtained. *These estimates are expressed as* [15]

$$\widehat{u}_m(n_x) = \mu_m + n_x\frac{\lambda}{D_x} \tag{21}$$

$$\left\lceil \frac{D_x}{\lambda}(-0.5 - \mu_m) \right\rceil \le n_x \le \left\lfloor \frac{D}{\lambda}(0.5 - \mu_m) \right\rfloor \tag{22}$$

$$\mu_m = \frac{\arg\left(\left[\widehat{\boldsymbol{\Phi}}_u\right]_{m,m}\right)}{2\pi D_x/\lambda} \tag{23}$$

Similarly, we can obtain a set of cyclically ambiguous direction cosine estimates $\nu_m$ from the data block $\boldsymbol{R}_y$. These estimates are expressed as [15]

$$\widehat{\nu}_m(n_y) = \nu_m + n_y\frac{\lambda}{D_y} \tag{24}$$

$$\left\lceil \frac{D_y}{\lambda}(-0.5 - \nu_m) \right\rceil \le n_y \le \left\lfloor \frac{D_y}{\lambda}(0.5 - \nu_m) \right\rfloor \tag{25}$$

$$\nu_m = \frac{\arg\left(\left[\widehat{\boldsymbol{\Phi}}_v\right]_{m,m}\right)}{2\pi D_y/\lambda} \tag{26}$$

where $\{[\widehat{\boldsymbol{\Phi}}_v]_{m,m} = e^{j2\pi/\lambda D_y \widehat{\nu}_m},\ m = 1, 2, \ldots, M\}$.

The above low-variance but cyclically ambiguous direction cosine estimates can be disambiguated by using the set of high-variance but unambiguous direction cosine estimates extracted from the estimation of electromagnetic vector sensor array manifolds. This extraction may be accomplished by decoupling the matrix $\widehat{\boldsymbol{A}}$ as

$$\widehat{\boldsymbol{C}}_0 = \frac{\sum_{\ell=1}^{\overline{L}}\widehat{\boldsymbol{A}}_\ell}{\left\|\sum_{\ell=1}^{\overline{L}}\widehat{\boldsymbol{A}}_\ell\right\|_F} \tag{27}$$

where $\widehat{\boldsymbol{A}}_\ell$ denotes the $((\ell-1)\times 6+1)$th to $(\ell\times 6)$th elements of $\widehat{\boldsymbol{A}}$. According to (18), $\widehat{\boldsymbol{A}}$ can be estimated as the first $6\overline{L}$ rows of $\widehat{\boldsymbol{E}}_{s,x}\widehat{\boldsymbol{T}}^{-1}$. Denoting the $m$th column of $\widehat{\boldsymbol{C}}_0$ as $g\widehat{\boldsymbol{c}}_m$, the high-variance but unambiguous direction cosine estimates of the $m$th signal can be directly calculated by the vector cross product between the normalized electric field vector and the magnetic field vector, i.e.,

$$\widehat{\boldsymbol{p}}_m = \begin{bmatrix} \widehat{u}_m^{\mathrm{ref}} \\ \widehat{v}_m^{\mathrm{ref}} \\ \widehat{w}_m^{\mathrm{ref}} \end{bmatrix} = \frac{\widehat{\boldsymbol{e}}_m}{\left\|\widehat{\boldsymbol{e}}_m\right\|} \times \frac{\widehat{\boldsymbol{h}}_m^H}{\left\|\widehat{\boldsymbol{h}}_m\right\|} \tag{28}$$

where $\widehat{\boldsymbol{e}}_m$ and $\widehat{\boldsymbol{h}}_m$, respectively, correspond to the first three and the last three columns of $g\widehat{\boldsymbol{c}}_m$.

Finally, the high-variance but unambiguous direction cosine estimates $(\widehat{u}_m^{\text{ref}}, \widehat{v}_m^{\text{ref}})$, $m = 1, \ldots, M$ would serve as reference direction cosine estimates to resolve the cyclically ambiguous direction cosines estimates $(\widehat{u}_m(n_x), \widehat{v}_m(n_y))$, $m = 1, \ldots, M$. The disambiguated $x$-axis and $y$-axis direction cosines, $\widehat{u}_m$ and $\widehat{v}_m$, are found from $\widehat{u}_m(n_x)$ and $\widehat{v}_m(n_y)$ when the value of $|\widehat{u}_m(n_x) - \widehat{u}_m^{\text{ref}}|$ and $|\widehat{v}_m(n_y) - \widehat{v}_m^{\text{ref}}|$ are minimized. Mathematically, the disambiguated $x$-axis direction cosine estimates $\widehat{u}_m$ are given by

$$\widehat{u}_m = \mu_m + n_x^o \frac{\lambda}{D} \tag{29}$$

where $n_x^o$ is estimated as

$$n_x^o = \underset{n_x}{\operatorname{argmin}} \left| \widehat{u}_m^{\text{ref}} - \mu_m - \frac{n_x \lambda}{D} \right| \tag{30}$$

Analogously, the disambiguated $y$-axis direction cosine estimates $\widehat{v}_m$ are

$$\widehat{v}_m = \nu_m + n_y^o \frac{\lambda}{D} \tag{31}$$

where $n_y^o$ is estimated as

$$n_y^o = \underset{n_y}{\operatorname{argmin}} \left| \widehat{v}_m^{\text{ref}} - \nu_m - \frac{n_y \lambda}{D} \right| \tag{32}$$

Note that since $\widehat{u}_m^{\text{ref}}$ is paired with $\widehat{v}_m^{\text{ref}}$, the estimated $\widehat{u}_m$ and $\widehat{v}_m$ are then automatically paired without any additional processing.

*3.3. Implementation of the MIMED Algorithm.* The implementation of the proposed MIMED algorithm is summarized as follows:

(S1) Estimate the cumulant matrices $\widehat{\boldsymbol{R}}_\ell$, $\ell = 1, \ldots, \overline{L}$, from the data samples.

(S2) Form the matrices $\widehat{\boldsymbol{R}}_x$ and $\widehat{\boldsymbol{R}}_y$ using (16); then perform the eigenvalue decomposition to $\widehat{\boldsymbol{R}}_x \widehat{\boldsymbol{R}}_x^H$ and $\widehat{\boldsymbol{R}}_y \widehat{\boldsymbol{R}}_y^H$ to construct the signal subspaces $\widehat{\boldsymbol{E}}_{s,x}$ and $\widehat{\boldsymbol{E}}_{s,y}$, whose columns correspond to the eigenvectors associated with $M$ largest eigenvalues of $\widehat{\boldsymbol{E}}_{s,x}$ and $\widehat{\boldsymbol{E}}_{s,y}$.

(S3) Let $\widehat{\boldsymbol{E}}_{s,x,1}$ and $\widehat{\boldsymbol{E}}_{s,x,2}$, respectively, be the first $6L\overline{L}$ rows and the last $6L\overline{L}$ rows of $\widehat{\boldsymbol{E}}_{s,x}$, $\widehat{\boldsymbol{E}}_{s,y,1}$, and $\widehat{\boldsymbol{E}}_{s,y,2}$, respectively, be the first $6L\overline{L}$ rows and the last $6L\overline{L}$ rows of $\widehat{\boldsymbol{E}}_{s,y}$. Perform eigenvalue decomposition of $\widehat{\boldsymbol{E}}_{s,x,1}^{\dagger} \widehat{\boldsymbol{E}}_{s,x,2}$ and $\widehat{\boldsymbol{E}}_{s,y,1}^{\dagger} \widehat{\boldsymbol{E}}_{s,y,2}$.

(S4) Estimate the ambiguous direction cosine estimates $\widehat{u}_m(n_x)$ and $\widehat{v}_m(n_y)$ from (21) to (23) and (24) to (26).

(S5) Estimate $\widehat{\boldsymbol{C}}_0$ using (27).

(S6) Compute reference direction cosine estimates $\widehat{u}_m^{\text{ref}}$ and $\widehat{v}_m^{\text{ref}}$ using (28).

(S7) Obtain the disambiguated direction cosine estimates $\widehat{u}_m$ and $\widehat{v}_m$ using (29) and (31).

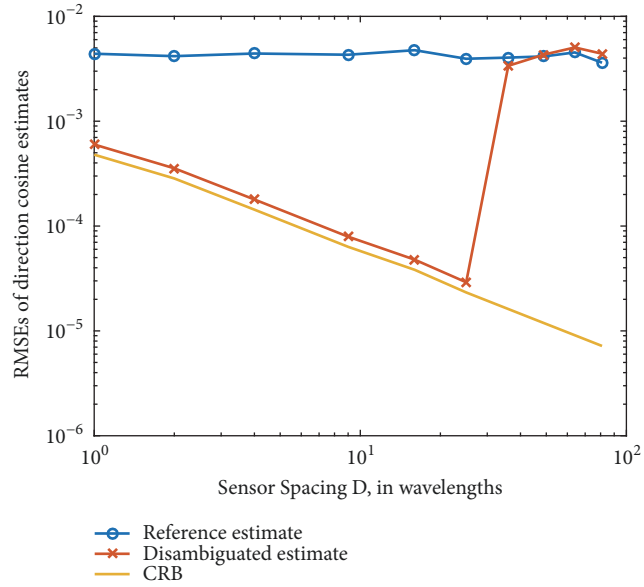


Figure 2: RMSEs of the direction cosine estimates versus intersensor spacing, varying from $1\lambda$ to $81\lambda$. SNR = 20 dB. Two monochromatic signals with digital frequencies $f_1 = 0.1$, $f_2 = 0.4$ and direction cosines $u_1 = 0.3$ and $v_1 = 0.2$ and $u_2 = 0.43$ and $v_2 = 0.35$ impinge upon the array.

## 4. Simulation Results

Simulation results are presented to demonstrate the efficacy of the MIMED. The array configuration in Figure 1 with $\overline{L} = 15$ elements is used. Two narrowband uncorrelated monochromatic signals with identical power impinge on the array. The signal direction cosines $u_1 = 0.3$, $v_1 = 0.2$, $u_2 = 0.43$, and $v_2 = 0.35$ are simulated. The first signal is left-circularly polarized and the second right-circularly polarized. The snapshots used are $N = 200$ snapshots. 500 independent Monte Carlo trials are performed. Further the additive white noise is assumed to be complex Gaussian. In all the simulations, the performance metric used is the root mean squared error (RMSE) of the first signal.

We first assess the performance of the MIMED for various values of $D_x = D_y = D$, the intersensor spacing. Figure 2 shows, on a log-log scale, the RMSEs of the reference direction estimates $(\widehat{\theta}_1^{\text{ref}}, \widehat{\phi}_1^{\text{ref}})$ and the disambiguated direction estimates $(\widehat{\theta}_1, \widehat{\phi}_1)$ as a function of $D$, varying from $1\lambda$ to $81\lambda$, $\lambda$ being the wavelength. The SNR for each of the signals is set to 20dB. It is seen that the RMSE of the disambiguated direction estimates decrease linearly as the intersensor spacing increases from $1\lambda$ up to $25\lambda$. The performance of the reference direction estimates keeps almost unchanged as the sensor spacing increases from $1\lambda$ to $81\lambda$. For $D > 36\lambda$, the disambiguated direction estimates exhibit almost the same statistical errors as the reference direction estimates. This behavior is similar to that in [4] and can be explained as follows. Referring to (29) and (31), the estimates $u_1(n_x)$ and $v_1(n_y)$ suffer ambiguities of some unknown integer multiples of the grid size $\lambda/D$. As the intersensor spacing $D$ increases, the grid sizes shrink relative to the variances of the reference

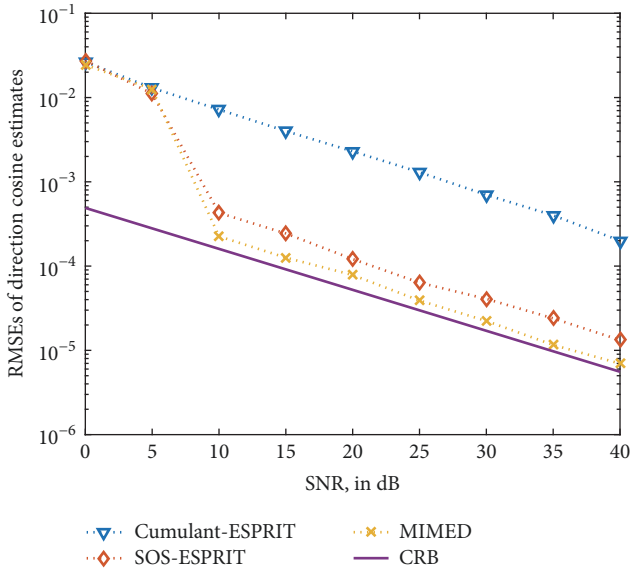


Figure 3: RMSEs of the direction cosine estimates versus SNR. Two monochromatic signals with digital frequencies $f_1 = 0.1, f_2 = 0.4$ and direction cosines $u_1 = 0.3$ and $v_1 = 0.2$ and $u_2 = 0.43$ and $v_2 = 0.35$ impinge upon the array.

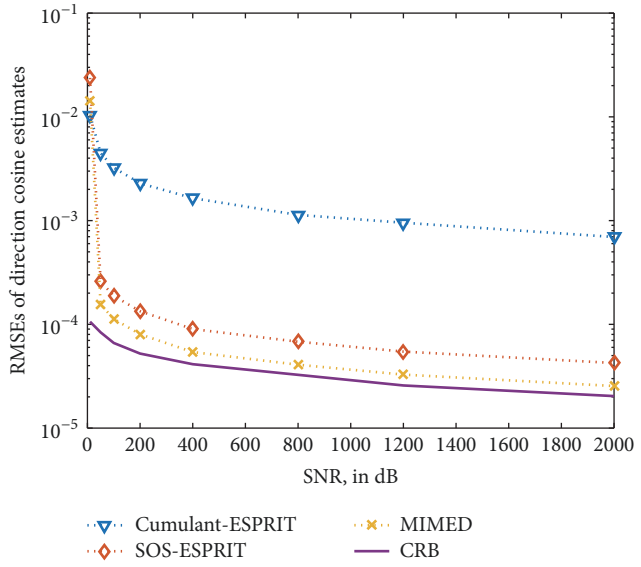


Figure 4: RMSEs of the direction cosine estimates versus snapshot number. Two monochromatic signals with digital frequencies $f_1 = 0.1, f_2 = 0.4$ and direction cosines $u_1 = 0.3$ and $v_1 = 0.2$ and $u_2 = 0.43$ and $v_2 = 0.35$ impinge upon the array.

estimates $\widehat{u}_1^{\text{ref}}$ and $\widehat{v}_1^{\text{ref}}$. Therefore, it becomes increasingly probable that $\widehat{u}_1^{\text{ref}}$ and $\widehat{v}_1^{\text{ref}}$ would identify the wrong grid point. As the intersensor spacing continues to increase, the grid misidentification will become the dominant error, and the disambiguated estimates $\widehat{u}_1$ and $\widehat{v}_1$ eventually have the same error statistics as the reference estimates $\widehat{u}_1^{\text{ref}}$ and $\widehat{v}_1^{\text{ref}}$. These imply that $\widehat{\theta}_1$ and $\widehat{\phi}_1$ would have the same error statistics as $\widehat{\theta}_1^{\text{ref}}$ and $\widehat{\phi}_1^{\text{ref}}$. Also note that the performance of the MIMED algorithm is very close to the CRB.

In the second example, we compare the RMSEs of the MIMED with the cumulant-based ESPRIT algorithm proposed by Liu and Mendel [16] and the second-order statistics based ESPRIT-based algorithm proposed by Zoltowski and Wong [4]. For the algorithm in [16], we assume 96-element arbitrarily-spaced array configuration that contains three presets guiding sensors located at $(0, 0)$, $(\lambda/2, 0)$, and $(0, \lambda/2)$. For the algorithm in [4], we use a 16-element square-shaped electromagnetic vector sensor array. For these two algorithms, the estimated sets of directions are assumed to have been correctly paired. For the MIMED and the one in [4], we set $D = 5\lambda$. Figure 3 shows the RMSEs of the three algorithms as a function of the SNR, varying from 0 dB to 40 dB. It is seen from the figure that the MIMED has a performance that is better than those of the other two algorithms for a wide range of the SNR (SNR > 10dB).

In the third example, we compare the RMSEs of the algorithms as a function of the number of snapshots. The simulation conditions are similar to those in the second example, except that the SNR is set at 20 dB, and the number of snapshots is varying from 10 to 2000. The RMSEs of the three algorithms are shown in Figure 4, where the CRBs are also plotted for comparison. It is seen from the figure that the RMSEs of the MIMED algorithm are lower than those of the other two algorithms and are close to the CRBs.

## 5. Conclusions

We have presented a MIMED method for finding directions of non-Gaussian signals using cumulants. By using an array containing sparse $L$-shaped diversely polarized vector sensors plus an arbitrarily-placed single polarized scalar sensor, we have defined a set of cumulant matrices to construct two matrix blocks with multi-invariance property. We have then developed a MI-ESPRIT-based algorithm using the defined matrix blocks to estimate two-dimensional directions of the signals. The MIMED extends the array aperture by being able to space the sensors much farther apart than a half-wavelength.

## Data Availability

The data that support the findings of this study are available from the corresponding author upon reasonable request.

## Conflicts of Interest

The authors declare that there are no conflicts of interest regarding the publication of this paper.

## Acknowledgments

This work was supported in part by the National Natural Science Foundation of China under Grant 81601568, in part by the National Key Technology Support Program 2015BAI02B04, in part by the Natural Science Foundation of

Jiangsu Province under Grant SBK2014043201, and in part by the Fundamental Research Funds for the Central Universities under Grant 30917011316.

## References

[1] A. Nehorai and E. Paldi, "Vector-sensor array processing for electromagnetic source localization," *IEEE Transactions on Signal Processing*, vol. 42, no. 2, pp. 376–398, 1994.

[2] K. T. Wong and M. D. Zoltowski, "Uni-vector-sensor ESPRIT for multisource azimuth, elevation, and polarization estimation," *IEEE Transactions on Antennas and Propagation*, vol. 45, no. 10, pp. 1467–1474, 1997.

[3] K. T. Wong and M. D. Zoltowski, "Closed-form direction finding and polarization estimation with arbitrarily spaced electromagnetic vector-sensors at unknown locations," *IEEE Transactions on Antennas and Propagation*, vol. 48, no. 5, pp. 671–681, 2000.

[4] M. D. Zoltowski and K. T. Wong, "ESPRIT-based 2-D direction finding with a sparse uniform array of electromagnetic vector sensors," *IEEE Transactions on Signal Processing*, vol. 48, no. 8, pp. 2195–2204, 2000.

[5] K. T. Wong and M. D. Zoltowski, "Self-initiating MUSIC based direction finding and polarization estimation in spatio-polarizational beamspace," *IEEE Transactions on Antennas and Propagation*, vol. 48, no. 8, pp. 1235–1245, 2000.

[6] K. T. Wong, L. Li, and M. D. Zoltowski, "Root-MUSIC-based direction-finding and polarization-estimation using diversely-polarized possibly-collocated antennas," *IEEE Antennas and Wireless Propagation Letters*, vol. 3, no. 1, pp. 129–132, 2004.

[7] J. He, S. L. Jiang, J. T. Wang, and Z. Liu, "Polarization difference smoothing for direction finding of coherent signals," *IEEE Transactions on Aerospace and Electronic Systems*, vol. 46, no. 1, pp. 469–480, 2010.

[8] G. Zheng and B. Wu, "Polarisation smoothing for coherent source direction finding with multiple-input and multiple-output electromagnetic vector sensor array," *IET Signal Processing*, vol. 10, no. 8, pp. 873–879, 2016.

[9] A. L. Swindlehurst, B. Ottersten, R. Roy, and T. Kailath, "Multiple invariance ESPRIT," *IEEE Transactions on Signal Processing*, vol. 40, no. 4, pp. 867–881, 1992.

[10] X. Zhang, X. Gao, and D. Xu, "Multi-invariance ESPRIT-based blind DOA estimation for MC-CDMA with an antenna array," *IEEE Transactions on Vehicular Technology*, vol. 58, no. 8, pp. 4686–4690, 2009.

[11] Y. Xu and Z. Liu, "Noncircularity restoral for multi-antenna blind beamforming," *Multidimensional Systems and Signal Processing*, vol. 21, no. 2, pp. 133–160, 2010.

[12] J. Lin, X. Ma, S. Yan, and C. Hao, "Time-frequency multi-invariance ESPRIT for DOA estimation," *IEEE Antennas and Wireless Propagation Letters*, vol. 15, pp. 770–773, 2016.

[13] C. Gu, H. Hong, X. Zhu, and J. He, "Highly accurate two-dimensional direction finding using cumulant," *IEEE Access*, vol. 6, pp. 70910–70918, 2018.

[14] J. M. Mendel, "Tutorial on higher-order statistics (spectra) in signal processing and system theory: theoretical results and some applications," *Proceedings of the IEEE*, vol. 79, no. 3, pp. 278–305, 1991.

[15] J. He and Z. Liu, "Extended aperture 2-D direction finding with a two-parallel-shape-array using propagator method," *IEEE Antennas and Wireless Propagation Letters*, vol. 8, pp. 323–327, 2009.

[16] T.-H. Liu and J. M. Mendel, "Azimuth and elevation direction finding using arbitrary array geometries," *IEEE Transactions on Signal Processing*, vol. 46, no. 7, pp. 2061–2065, 1998.